Journal of Computational Physics **160,** 720–742 (2000)
doi:10.1006/jcph.2000.6485, available online at http://www.idealibrary.com on IDEAL®

New High-Resolution Semi-discrete Central Schemes for Hamilton–Jacobi Equations

Alexander Kurganov* and Eitan Tadmor†

**Department of Mathematics, University of Michigan, Ann Arbor, Michigan 48109; †Department of Mathematics, University of California at Los Angeles, Los Angeles, California 90095*
E-mail: kurganov@math.lsa.umich.edu, tadmor@math.ucla.edu

Received July 27, 1999; revised February 28, 2000

We introduce a new high-resolution central scheme for multidimensional Hamilton–Jacobi equations. The scheme retains the simplicity of the non-oscillatory central schemes developed by C.-T. Lin and E. Tadmor (in press, *SIAM J. Sci. Comput.*), yet it enjoys a smaller amount of numerical viscosity, independent of $1/\Delta t$. By letting $\Delta t \downarrow 0$ we obtain a new second-order central scheme in the particularly simple semi-discrete form, along the lines of the new semi-discrete central schemes recently introduced by the authors in the context of hyperbolic conservation laws. Fully discrete versions are obtained with appropriate Runge–Kutta solvers. The smaller amount of dissipation enables efficient integration of convection-diffusion equations, where the accumulated error is independent of a small time step dictated by the CFL limitation. The scheme is non-oscillatory thanks to the use of nonlinear limiters. Here we advocate the use of such limiters on *second discrete derivatives*, which is shown to yield an improved high resolution when compared to the usual limitation of first derivatives. Numerical experiments demonstrate the remarkable resolution obtained by the proposed new central scheme.

Key Words: multidimensional Hamilton–Jacobi equations; semi-discrete central schemes; high resolution; non-oscillatory time differencing.

CONTENTS

0021-9991/00 $35.00

1. INTRODUCTION

We consider the multidimensional Hamilton–Jacobi (HJ) equation with *Hamiltonian* H,

$$\varphi_t + H(\nabla_x \varphi) = 0, \tag{1.1}$$

where $x = (x_1, \ldots, x_d)$ are d-spatial variables.

These equations—with and without additional diffusive terms—are of practical importance with applications ranging from mathematical finance and differential games to front propagation and image enhancement. Consult [2] and the references therein for a recent bird's eye view on the theory of viscosity solutions and various applications, and [1, 6, 7, 13, 19, 20, 22, 24] for their approximate solution.

In this work we present new second-order central difference approximations to (1.1). These new schemes can be viewed as modifications of the central schemes of Lin and Tadmor (LT) [19, 20] and as an extension of the method developed by the authors in [15] for hyperbolic conservation laws and convection-diffusion equations.

The new schemes have a smaller amount of numerical viscosity than the LT schemes, and unlike the LT schemes, they can be written and integrated in the semi-discrete form. This allows us to efficiently solve not only Eqs. (1.1), but also viscous HJ equations of the form

$$\varphi_t + H(\nabla_x \varphi) = \varepsilon \Delta \varphi. \tag{1.2}$$

Semi-discrete schemes are especially effective when they combine *high-resolution, non-oscillatory spatial discretization* with high-order, large stepsize ODE solvers for their time evolution. In addition to being effective as a simple-to-use yet high-resolution solver, the semi-discrete formulation enables long term integration in the presence of degenerate diffusion, as outlined in, e.g., [15, Section 6.4].

The paper is organized as follows. In Section 2 we provide a brief description of the central differencing approach for HJ equations.

In Section 3 we introduce our main idea by constructing the new first-order semi-discrete central scheme for (1.1). Then our scheme is extended to the second-order one- (Section 4) and multidimensional (Section 5) schemes.

We conclude in Section 6 by presenting a number of numerical results. These results are convincing illustrations that our new central schemes provide high resolution.

2. CENTRAL SCHEMES FOR HAMILTON–JACOBI EQUATIONS—A BRIEF OVERVIEW

Central schemes can be viewed as Godunov-type projection-evolution methods—starting with point-values at time level t^n, one reconstructs a piecewise polynomial interpolant, which is evolved to the next time level t^{n+1}, and then it is being realized by its pointwise projection. The main feature of central schemes is *simplicity*, since no upwinding is involved in the evolution operator. We illustrate this central approach on the example of the one-dimensional second-order LT scheme [20].

Let φ_j^n denote an approximate value of $\varphi(x = x_j, t = t^n)$ at the grid point ($x_j := j\Delta x$, $t^n := n\Delta t$). Assume that we have computed the values of φ_j^n at time level t^n. Then we first

construct a continuous piecewise quadratic spatial interpolant,

$$\tilde{\varphi}(x,t^n) := \varphi_j^n + \frac{(\Delta\varphi)^n_{j+\frac{1}{2}}}{\Delta x}(x-x_j) + \frac{(\Delta\varphi)'_{j+\frac{1}{2}}}{2(\Delta x)^2}(x-x_j)(x-x_{j+1}), \tag{2.1}$$

which is a second-order approximation of $\varphi(x,t^n)$ on the corresponding interval $I_{j+1/2} := [x_j, x_{j+1}]$. Here, $(\Delta\varphi)^n_{j+1/2}/\Delta x$ denotes the usual approximation to the first derivative $\varphi_x(x_{j+1/2}, t^n)$, namely,

$$\frac{(\Delta\varphi)^n_{j+\frac{1}{2}}}{\Delta x} := \frac{\varphi^n_{j+1} - \varphi^n_j}{\Delta x}.$$

Similarly, $(\Delta\varphi)'_{j+1/2}/(\Delta x)^2$ is an approximation to the second derivative $\varphi_{xx}(x_{j+1/2}, t^n)$, where the prime $(\cdot)'$ indicates a numerical derivative. An appropriate *nonlinear limiter*, employed in this approximation guarantees the non-oscillatory behavior of the central scheme. There is a wide variety of such limiters, which were developed in the context of hyperbolic conservation laws (see, e.g., [9, 10, 14, 21, 23]). For instance, for an arbitrary grid function $\{w_{j+1/2}\}$ one may choose any limiter from the following one-parameter family of the *minmod* limiters [9, 17, 23],

$$w'_{j+\frac{1}{2}} = \operatorname{minmod}\left(\theta\left(w_{j+\frac{3}{2}} - w_{j+\frac{1}{2}}\right), \frac{1}{2}\left(w_{j+\frac{3}{2}} - w_{j-\frac{1}{2}}\right), \theta\left(w_{j+\frac{1}{2}} - w_{j-\frac{1}{2}}\right)\right), \tag{2.2}$$

where $\theta \in [1,2]$ and the multivariable minmod function is defined by

$$\operatorname{minmod}(x_1, x_2, \ldots) := \begin{cases} \min_j\{x_j\}, & \text{if } x_j > 0 \quad \forall j, \\ \max_j\{x_j\}, & \text{if } x_j < 0 \quad \forall j, \\ 0, & \text{otherwise.} \end{cases} \tag{2.3}$$

We note that if $\theta = 1$, then $w'_{j+1/2}$ does not exceed $|\Delta_\pm w_{j+1/2}/\Delta x|$ and therefore

$$\frac{(\Delta\varphi)'_{j+\frac{1}{2}}}{(\Delta x)^2} \sim \min\left(\left|\frac{\Delta^2\varphi_j}{(\Delta x)^2}\right|, \left|\frac{\Delta^2\varphi_{j+1}}{(\Delta x)^2}\right|\right), \tag{2.4}$$

which is the usual approximation to second derivatives. The virtue of (2.2) is the presence of the parameter θ—larger θ's correspond to less dissipative, but still *non-oscillatory* limiters [9, 17, 23]. The quantity on the right of (2.4) represents yet another possible limiter—a limiter based on the differentiated second-order ENO interpolant which was introduced in the context approximate HJ solutions by Osher and Shu [22]. We note in passing that this ENO limiter differs from the minmod on the right of (2.4) only at inflection points, where the latter vanishes. The fact minmod values vanish at inflection points guarantees the maximum principle in reconstruction of $\tilde{\varphi}_x$, which otherwise fails with the ENO limiter.

At the second step of this projection-evolution method, the quadratic interpolant, reconstructed in (2.1), is evolved exactly in time and is realized by its point-value projection at $(x_{j+1/2}, t^{n+1})$ resulting in

$$\varphi^{n+1}_{j+\frac{1}{2}} = \tilde{\varphi}\left(x_{j+\frac{1}{2}}, t^n\right) - \int_{t^n}^{t^{n+1}} H\left(\varphi_x\left(x_{j+\frac{1}{2}}, t\right)\right) dt. \tag{2.5}$$

Our continuous interpolant may be nonsmooth at the grid points, x_j; yet for Δt sufficiently small (so that a CFL condition, $\frac{\Delta t}{\Delta x}\max|H'| \le \frac{1}{2}$, holds) the solution of the initial value problem (1.1)–(2.1) will remain smooth around $x_{j+1/2}$ for $t \le t^n + \Delta t =: t^{n+1}$, due to the finite speed of propagation. Hence, the integral on the RHS of (2.5) can be approximated by the midpoint rule.

To this end, the required midpoint value of $(\varphi_x)^{n+1/2}_{j+1/2} := \varphi_x(x_{j+1/2}, t^{n+1/2})$ can be predicted by the Taylor expansion,

$$(\varphi_x)^{n+\frac{1}{2}}_{j+\frac{1}{2}} = \frac{(\Delta\varphi)^n_{j+\frac{1}{2}}}{\Delta x} - \frac{\Delta t}{2}\cdot H'\left(\frac{(\Delta\varphi)^n_{j+\frac{1}{2}}}{\Delta x}\right)\cdot\frac{(\Delta\varphi)'_{j+\frac{1}{2}}}{(\Delta x)^2}. \tag{2.6}$$

Inserting (2.6) into (2.5) results in the following second-order *staggered* scheme,

$$\varphi^{n+1}_{j+\frac{1}{2}} = \frac{1}{2}\left(\varphi^n_j + \varphi^n_{j+1}\right) - \frac{1}{8}(\Delta\varphi)'_{j+\frac{1}{2}} - \Delta t\cdot H\left((\varphi_x)^{n+\frac{1}{2}}_{j+\frac{1}{2}}\right). \tag{2.7}$$

This concludes the two-step construction of the second-order, central LT scheme, (2.6)–(2.7), which is graphically described in Fig. 2.1. A two-dimensional extension of this scheme can be found in [20].

Remarks. (1) In the particular case of $(\Delta\varphi)'_{j+1/2} \equiv 0$, the second-order LT scheme is reduced to the staggered form of the first-order LxF scheme,

$$\varphi^{n+1}_{j+\frac{1}{2}} = \frac{1}{2}\left(\varphi^n_j + \varphi^n_{j+1}\right) - \Delta t\cdot H\left(\frac{(\Delta\varphi)^n_{j+\frac{1}{2}}}{\Delta x}\right). \tag{2.8}$$

(2) Compared with the LxF scheme, the second-order LT scheme provides much better resolution of nonsmooth solutions. This is due to the lower amount of numerical dissipation—considerably lower than in the first-order LxF scheme (the numerical viscosity present in a staggered central scheme is of order $\mathcal{O}((\Delta x)^{2r}/\Delta t)$, where r is its formal order of accuracy). However, if we are enforced to use the LT scheme with small time steps (e.g., due to a more restrictive CFL condition associated with the viscous HJ equation, (1.2)), then excessive numerical dissipation—of order $\mathcal{O}((\Delta x)^{2r}/\Delta t)$, will be accumulated. The effect of such accumulated dissipation also makes central schemes inappropriate for steady-state calculations as $t \uparrow \infty$ (consult the discussion in [15, Sect. 2]).

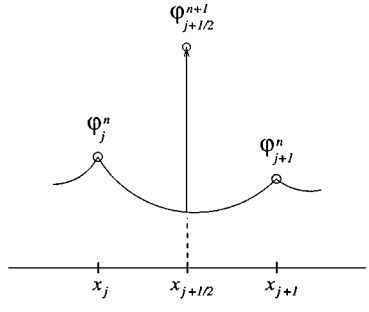

FIG. 2.1. Central differencing approach.

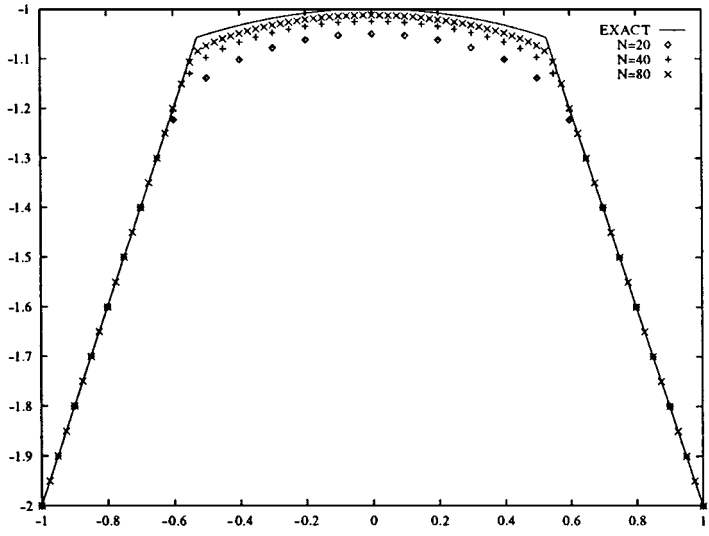

FIG. 2.2. Problem (6.4), $\mathbf{T} = \mathbf{1}$. Resolution via the modified LT scheme, (2.6)–(2.7), with limiters applied to second derivatives.

Our new central schemes introduced in the next three sections have a considerably smaller numerical dissipation of order $\mathcal{O}((\Delta x)^{2r-1})$. In particular, this allows us to compute the semi-discrete limit as $\Delta t \downarrow 0$.

(3) In fact, the scheme (2.6)–(2.7) is a modified version of the original LT scheme presented in [19]. Here we use the minmod (or any other nonlinear) limiter to approximate the second derivative, φ_{xx}, instead of limiting the first derivative, φ_x, as in [19]. We would like to emphasize that in [19, 20] the second derivative was approximated by $\Delta(\varphi')_{j+1/2}/(\Delta x)^2$, while here we use a different approximation, $(\Delta\varphi)'_{j+1/2}/(\Delta x)^2$, and that due to the nonlinearity of the limiter (2.2),

$$\Delta(\varphi')_{j+\frac{1}{2}} := \varphi'_{j+1} - \varphi'_j \neq (\Delta\varphi)'_{j+\frac{1}{2}} := (\varphi_{j+1} - \varphi_j)'.$$

Note that a typical solution of a HJ equation is continuous, but its first derivatives may be discontinuous. Consequently, limiting second derivatives seems to be the correct approach which significantly decreases the amount of numerical dissipation. Indeed, limiting second discrete derivatives was already used in [22], using the ENO limiter recorded on the right of (2.4). The improvement can be clearly seen even in the one-dimensional case. For instance, consider the Riemann problem (6.4) (from Example 2 below) and compare the numerical results obtained by the modified LT scheme, (2.6)–(2.7), and the original LT scheme [20], presented in Figs. 2.2 and 2.3.

3. THE ONE-DIMENSIONAL FIRST-ORDER SCHEME

The main idea in the construction of our new central schemes is to use more precise information about the *local* speed of propagation. We proceed along the lines of [15] as follows.

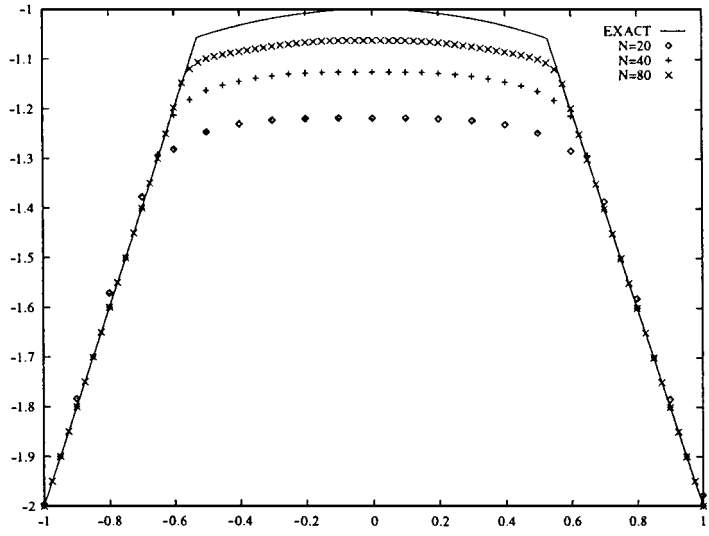

FIG. 2.3. Problem (6.4), $\mathbf{T}=\mathbf{1}$. Resolution via the original LT scheme [20], with limiters applied to first derivatives.

Assume that we have already computed the solution at time level t^n realized by its point-values, $\{\varphi_j^n\}$, and have reconstructed the continuous piecewise linear interpolant,

$$\tilde{\varphi}(x,t^n) := \sum_j \left[\varphi_j^n + \frac{(\Delta\varphi)^n_{j+\frac{1}{2}}}{\Delta x}(x-x_j)\right]\mathbf{1}_{[x_j,x_{j+1}]}. \tag{3.1}$$

We now turn to evolve it in time. To begin with, we estimate the local speed of propagation at the grid points, x_j: the upper bound (disregarding the direction of the propagation) is denoted by a_j^n and is given by

$$a_j^n := \max_{p\in[\tilde{\varphi}_x(x_j+0,t^n),\,\tilde{\varphi}_x(x_j-0,t^n)]} |H'(p)|. \tag{3.2}$$

Remark. In most practical applications, these local maximal speeds can be easily evaluated. For example, in the special case of convex Hamiltonian one finds that (3.2) reduces to

$$a_j^n = \max_{\pm}\left|H'\left(\frac{(\Delta\varphi)^n_{j\pm\frac{1}{2}}}{\Delta x}\right)\right|. \tag{3.3}$$

In fact, the local speeds are already calculated towards the CFL number, $\frac{\Delta t}{\Delta x}\max_j a_j^n$. We emphasize that these local speeds are the only additional information required to modify the LT scheme.

Our new scheme is constructed in two steps. First, we evolve in time the values of φ at the points x^n_{j+} and x^n_{j-}; see Fig. 3.1. Due to the finite speed of propagation these points, $x^n_{j\pm} := x_j \pm a_j^n\Delta t$, separate between smooth and nonsmooth regions, and hence the solution remains smooth along $(x^n_{j\pm}, t)$ with $t\in[t^n, t^{n+1}]$. Taylor expansion then yields

$$\varphi^{n+1}_{j\pm} = \tilde{\varphi}(x_{j\pm}, t^n) - \Delta t\cdot H\left(\frac{(\Delta\varphi)^n_{j\pm\frac{1}{2}}}{\Delta x}\right), \tag{3.4}$$

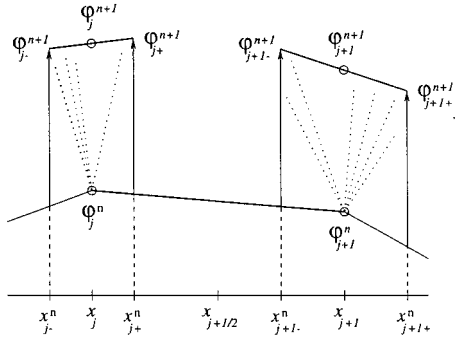

FIG. 3.1. Modified central differencing.

where the corresponding values at time t^n are computed directly from the interpolant (3.1),

$$\tilde{\varphi}(x_{j\pm}, t^n) = \varphi_j^n \pm \frac{\Delta t}{\Delta x} a_j^n (\Delta\varphi)^n_{j\pm\frac{1}{2}}. \tag{3.5}$$

Finally, the point-value of our approximation at (x_j, t^{n+1}) is obtained from the linear interpolation between $\varphi^{n+1}_{j\pm}$; i.e., noting that $x_j = \frac{1}{2}(x^n_{j+} + x^n_{j-})$ we conclude with

$$\begin{aligned}\varphi_j^{n+1} = \frac{1}{2}\left(\varphi^{n+1}_{j+} + \varphi^{n+1}_{j-}\right) = \varphi_j^n - \frac{\Delta t}{2}\left[H\left(\frac{(\Delta\varphi)^n_{j+\frac{1}{2}}}{\Delta x}\right) + H\left(\frac{(\Delta\varphi)^n_{j-\frac{1}{2}}}{\Delta x}\right)\right] \\ + \frac{\Delta t}{2\Delta x} a_j^n\left(\varphi^n_{j+1} - 2\varphi^n_j + \varphi^n_{j-1}\right).\end{aligned} \tag{3.6}$$

This is our *fully discrete* first-order scheme. Letting $\Delta t \downarrow 0$ yields the corresponding *semi-discrete* first-order scheme which reads

$$\begin{aligned}\frac{d}{dt}\varphi_j(t) = -\frac{1}{2}\left[H\left(\frac{(\Delta\varphi)_{j+\frac{1}{2}}(t)}{\Delta x}\right) + H\left(\frac{(\Delta\varphi)_{j-\frac{1}{2}}(t)}{\Delta x}\right)\right] \\ + \frac{a_j(t)}{2\Delta x}(\varphi_{j+1}(t) - 2\varphi_j(t) + \varphi_{j-1}(t)),\end{aligned} \tag{3.7}$$

where the $a_j(t)$ are the maximal local speeds

$$a_j(t) := \max_{p\in[\tilde{\varphi}_x(x_j+0,t),\tilde{\varphi}_x(x_j-0,t)]} |H'(p)|, \tag{3.8}$$

associated with the piecewise linear interpolant $\tilde{\varphi}(x,t)$, (3.1), reconstructed at time t.

Remarks. (1) Note that the fully discrete scheme, (3.6), is in fact the first-order forward Euler time differencing of the corresponding semi-discrete scheme, (3.7).

(2) The approach used here can be still viewed central differencing in the sense that no (approximate) Riemann solvers are involved. Consequently, we retain one of the main advantages of the central schemes—simplicity. At the same time, we have gained smaller numerical viscosity which is, in the fully discrete case, proportional to $\mathcal{O}(\Delta x)$ as opposed to the $\mathcal{O}((\Delta x)^2/\Delta t)$-size numerical viscosity of the LxF scheme.

4. THE ONE-DIMENSIONAL SECOND-ORDER SCHEME

We start again assuming that we have computed the solution at time t^n. Then, to increase the order of accuracy, we construct the continuous piecewise quadratic interpolant, (2.1),

$$\tilde{\varphi}(x,t^n) := \sum_j \left[\varphi_j^n + \frac{(\Delta\varphi)^n_{j+\frac{1}{2}}}{\Delta x}(x-x_j) + \frac{(\Delta\varphi)'_{j+\frac{1}{2}}}{2(\Delta x)^2}(x-x_j)(x-x_{j+1}) \right] \mathbf{1}_{[x_j,x_{j+1}]}.$$

The maximal local speed, a_j^n, is still given by (3.2); for example, in the convex case it reduces to (compare with (3.3))

$$a_j^n = \max_{\pm} \left| H'\left(\frac{(\Delta\varphi)^n_{j\pm\frac{1}{2}}}{\Delta x} \mp \frac{(\Delta\varphi)'_{j\pm\frac{1}{2}}}{2\Delta x} \right) \right|. \tag{4.1}$$

Similarly to the first-order scheme (Section 3), our new second-order scheme is constructed in two steps.

1. Evolution. First, we compute the solution at the points $x^n_{j\pm} = x_j \pm a_j^n \Delta t$ using the Taylor expansion of φ, which remains smooth along $(x^n_{j\pm}, t)$, $t < t^n + \Delta t$,

$$\varphi^{n+1}_{j\pm} = \tilde{\varphi}(x_{j\pm}, t^n) - \Delta t \cdot H\big(\tilde{\varphi}_x\big(x^n_{j\pm}, t^n\big)\big) + \mathcal{O}(\Delta t)^2. \tag{4.2}$$

Here, the corresponding values of $\tilde{\varphi}$ are computed directly from the piecewise quadratic interpolant (2.1),

$$\tilde{\varphi}(x_{j\pm}, t^n) = \varphi_j^n \pm \lambda a_j^n (\Delta\varphi)^n_{j\pm\frac{1}{2}} + \frac{\lambda a_j^n \big(\lambda a_j^n - 1\big)}{2} (\Delta\varphi)'_{j\pm\frac{1}{2}}, \qquad \lambda := \frac{\Delta t}{\Delta x}; \tag{4.3}$$

and similarly we obtain

$$\tilde{\varphi}_x\big(x^n_{j\pm}, t^n\big) = \frac{(\Delta\varphi)^n_{j\pm\frac{1}{2}}}{\Delta x} \mp \left(\frac{1}{2} - \lambda a_j^n\right) \frac{(\Delta\varphi)'_{j\pm\frac{1}{2}}}{\Delta x}. \tag{4.4}$$

2. Projection. Consider the nonuniform grid, $\{\cdots < x^n_{j-} < x^n_{j+} < x^n_{j+1-} < \cdots\}$; and the corresponding values of the computed approximate solution, $\{\varphi^{n+1}_{j\pm}\}$. We "tie" a continuous piecewise quadratic interpolant between these grid-values obtaining

$$\tilde{\phi}(x,t^{n+1}) := \sum_j \big\{ Q_j(x) \mathbf{1}_{[x^n_{j-}, x^n_{j+}]} + Q_{j+\frac{1}{2}}(x) \mathbf{1}_{[x^n_{j+}, x^n_{j+1-}]} \big\}. \tag{4.5}$$

Each quadratic part, $Q_j(x)$ or $Q_{j+1/2}(x)$, is of the form (2.1) and can be computed explicitly. Since our main goal is to construct a semi-discrete scheme, we omit these details.

We note that the support of $Q_j(x)$ is of size $x^n_{j+} - x^n_{j-} = \mathcal{O}(\Delta t)$, and hence we can safely replace $Q_j(x)$ by its linear interpolant modulo a negligible local error of order $\mathcal{O}(\Delta t)^2$, i.e.,

$$Q_j(x) = \varphi^{n+1}_{j-} + \frac{\varphi^{n+1}_{j+} - \varphi^{n+1}_{j-}}{2a_j^n \Delta t} \big(x - x^n_{j-}\big) + \mathcal{O}(\Delta t)^2. \tag{4.6}$$

Thus, we complete our fully discrete construction by inserting $x = x_j$ into (4.5) and (4.6) and using (4.2)–(4.3). the resulting scheme reads

$$\begin{aligned}\varphi_j^{n+1} &= \tilde{\phi}(x_j, t^{n+1}) = \frac{1}{2}\left(\varphi_{j+}^{n+1} + \varphi_{j-}^{n+1}\right) + \mathcal{O}(\Delta t)^2 \\ &= \varphi_j^n + \frac{\lambda a_j^n}{2}\left((\Delta\varphi)_{j+\frac{1}{2}}^n - (\Delta\varphi)_{j-\frac{1}{2}}^n\right) + \frac{\lambda a_j^n\left(\lambda a_j^n - 1\right)}{4}\left((\Delta\varphi)'_{j+\frac{1}{2}} + (\Delta\varphi)'_{j-\frac{1}{2}}\right) \\ &\quad - \frac{\Delta t}{2}\left[H\left(\varphi_x\left(x_{j+}^n, t^n\right)\right) + H\left(\varphi_x\left(x_{j-}^n, t^n\right)\right)\right] + \mathcal{O}(\Delta t)^2. \end{aligned} \tag{4.7}$$

The fully discrete scheme (4.7) is second-order in space and only first-order in time. This is attributed to the first-order forward Euler time differencing employed in (4.7), which we abbreviate as

$$\varphi^{n+1} = \varphi^n + \Delta t C[\varphi^n].$$

To gain second-order accuracy in time, one may use a modified Euler method (see, e.g., [25, 26]),

$$\varphi^{n+1} = \varphi^n + \Delta t C\left[\varphi^{n+\frac{1}{2}}\right], \qquad \varphi^{n+\frac{1}{2}} := \varphi^n + \frac{\Delta t}{2} C[\varphi^n]. \tag{4.8}$$

Yet a more compact and economical approach for higher accuracy in time would be based on a direct application of the semi-discrete form, associated with (4.7). It is here that we take advantage of the semi-discrete form available for our new central scheme (as opposed to the LT central scheme). Thus, letting $\Delta t \downarrow 0$ in (4.7) and (4.4), we arrive at the *semi-discrete second-order central scheme*, which takes the compact form,

$$\frac{d}{dt}\varphi_j(t) = -\frac{1}{2}[H(\varphi_x^+(t)) + H(\varphi_x^-(t))] + \frac{a_j(t)}{2}(\varphi_x^+(t) - \varphi_x^-(t)). \tag{4.9}$$

Here, $a_j(t)$ is given by (3.8), and all the quantities on the right are attached to the point x_j, namely

$$\varphi_x^{\pm}(t) := \tilde{\varphi}_x(x_j \pm 0, t) = \frac{(\Delta\varphi)_{j\pm\frac{1}{2}}(t)}{\Delta x} \mp \frac{(\Delta\varphi)'_{j\pm\frac{1}{2}}(t)}{2\Delta x}. \tag{4.10}$$

To achieve high-order accuracy in time, this semi-discrete scheme, (4.9)–(4.10) can be integrated in time by an appropriate high-order ODE solver; for example, the second-order modified Euler method (4.8) will do.

Remark. If we set all the numerical derivatives, $(\Delta\varphi)'_{j+\frac{1}{2}}(t)$, to be zero, our second-order semi-discrete scheme, (4.9)–(4.10), reduces to the first-order scheme, (3.7), introduced in Section 3.

5. THE MULTIDIMENSIONAL SECOND-ORDER SCHEME

Without loss of generality, we restrict our attention to $d = 2$ space dimensions, considering the HJ equation,

$$\varphi_t + H(\varphi_x, \varphi_y) = 0. \tag{5.1}$$

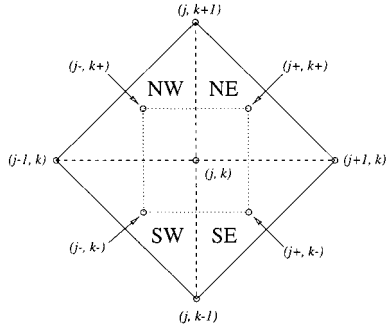

FIG. 5.1. Two-dimensional central differencing.

Assume that at time $t = t^n$ the discrete approximation to the point-values of its solution, $\{\varphi^n_{j,k} \approx \varphi(x_j := j\Delta x, y_k := k\Delta y, t^n)\}$, has been already computed. We begin with the reconstruction of a continuous, piecewise quadratic, two-dimensional interpolant in four triangles (NW, NE, SW, and SE) around each grid-point, (x_j, y_k) (see Fig. 5.1). Such an interpolant in the NE (NW) triangles is given by

$$\begin{aligned}\tilde{\varphi}^{\mathrm{NE(NW)}}(x,y) = \varphi^n_{j,k} &+ \frac{(\Delta\varphi)^n_{j\pm\frac{1}{2},k}}{\Delta x}(x - x_j) + \frac{(\Delta\varphi)^n_{j,k+\frac{1}{2}}}{\Delta y}(y - y_k)\\ &+ \frac{(\Delta\varphi)'_{j\pm\frac{1}{2},k}}{2(\Delta x)^2}(x - x_j)(x - x_{j\pm1}) + \frac{(\Delta\varphi)`_{j,k+\frac{1}{2}}}{2(\Delta y)^2}(y - y_k)(y - y_{k+1})\\ &+ \frac{(\Delta\varphi)'_{j,k+\frac{1}{2}} + (\Delta\varphi)`_{j\pm\frac{1}{2},k}}{2\Delta x\Delta y}(x - x_j)(y - y_k),\end{aligned} \tag{5.2}$$

and in the SE (SW) triangles by

$$\begin{aligned}\tilde{\varphi}^{\mathrm{SE(SW)}}(x,y) = \varphi^n_{j,k} &+ \frac{(\Delta\varphi)^n_{j\pm\frac{1}{2},k}}{\Delta x}(x - x_j) + \frac{(\Delta\varphi)^n_{j,k-\frac{1}{2}}}{\Delta y}(y - y_k)\\ &+ \frac{(\Delta\varphi)'_{j\pm\frac{1}{2},k}}{2(\Delta x)^2}(x - x_j)(x - x_{j\pm1}) + \frac{(\Delta\varphi)`_{j,k-\frac{1}{2}}}{2(\Delta y)^2}(y - y_k)(y - y_{k-1})\\ &+ \frac{(\Delta\varphi)'_{j,k-\frac{1}{2}} + (\Delta\varphi)`_{j\pm\frac{1}{2},k}}{2\Delta x\Delta y}(x - x_j)(y - y_k).\end{aligned} \tag{5.3}$$

Here and below, $(\Delta\varphi)^n_{j+1/2,k} := \varphi^n_{j+1,k} - \varphi^n_{j,k}$, $(\Delta\varphi)^n_{j,k+1/2} := \varphi^n_{j,k+1} - \varphi^n_{j,k}$; and

$$\frac{(\Delta\varphi)'_{j+\frac{1}{2},k}}{(\Delta x)^2}, \qquad \frac{(\Delta\varphi)'_{j,k+\frac{1}{2}}}{\Delta x\Delta y}, \qquad \frac{(\Delta\varphi)`_{j+\frac{1}{2},k}}{\Delta x\Delta y}, \qquad \frac{(\Delta\varphi)`_{j,k+\frac{1}{2}}}{(\Delta y)^2}$$

are approximations to the corresponding exact derivatives,

$$\varphi_{xx}\left(x_{j+\frac{1}{2}}, y_k, t^n\right), \qquad \varphi_{xy}\left(x_j, y_{k+\frac{1}{2}}, t^n\right), \qquad \varphi_{xy}\left(x_{j+\frac{1}{2}}, y_k, t^n\right), \qquad \varphi_{yy}\left(x_j, y_{k+\frac{1}{2}}, t^n\right),$$

which are *reconstructed* from the computed differences $\{(\Delta\varphi)^n_{j+1/2,k}, (\Delta\varphi)^n_{j,k+1/2}\}$ with the help of a nonlinear limiter, e.g., the minmod limiter, (2.2)–(2.3), applied in an appropriate

direction. For instance, we compute

$$(\Delta\varphi)^{\backprime}_{j+\frac12,k}=\operatorname{minmod}\Bigg(\theta\Big((\Delta\varphi)^n_{j+\frac12,k+1}-(\Delta\varphi)^n_{j+\frac12,k}\Big),\frac12\Big((\Delta\varphi)^n_{j+\frac12,k+1}-(\Delta\varphi)^n_{j+\frac12,k-1}\Big),$$
$$\theta\Big((\Delta\varphi)^n_{j+\frac12,k}-(\Delta\varphi)^n_{j+\frac12,k-1}\Big)\Bigg),$$
$$(\Delta\varphi)^{\backprime}_{j,k+\frac12}=\operatorname{minmod}\Bigg(\theta\Big((\Delta\varphi)^n_{j,k+\frac32}-(\Delta\varphi)^n_{j,k+\frac12}\Big),\frac12\Big((\Delta\varphi)^n_{j,k+\frac32}-(\Delta\varphi)^n_{j,k-\frac12}\Big),$$
$$\theta\Big((\Delta\varphi)^n_{j,k+\frac12}-(\Delta\varphi)^n_{j,k-\frac12}\Big)\Bigg).$$

Other numerical derivatives can be approximated in a similar manner.

Next, we denote by $a^n_{j,k}$ the maximal local speed of propagation at the grid-point (x_j, y_k), which is given by the maximal value over the square $C_{j,k}:=\{(x,y)\in[x_{j-1/2},x_{j+1/2}]\times[y_{k-1/2},y_{k+1/2}]\}$,

$$a^n_{j,k}:=\max_{C_{j,k}}\{|H_u(\tilde\varphi_x(x,y),\tilde\varphi_y(x,y))|,|H_v(\tilde\varphi_x(x,y),\tilde\varphi_y(x,y))|\}. \tag{5.4}$$

In practice, we used the maximal value over the four points $(x_{j\pm}, y_{k\pm})$, see Fig. 5.1,

$$a^n_{j,k}:=\max_{\pm}\Big\{\sqrt{H_u^2+H_v^2}\ \big|\ (\tilde\varphi_x(x_{j\pm},y_{k\pm}),\tilde\varphi_y(x_{j\pm},y_{k\pm}))\Big\}, \tag{5.5}$$

since $\tilde\varphi$ is continuous at the neighborhood of (x_j, y_k).

Equipped with the piecewise quadratic reconstruction, (5.2)–(5.3), and having the maximal local speeds, (5.5), we now can compute the discrete point-values of the solution at the next time level. As in the one-dimensional case, our two-dimensional scheme is constructed in two steps.

1. Evolution. First, we note that due to the finite speed of propagation, the solution of (5.1) subject to the initial data, (5.2)–(5.3), prescribed at time $t=t^n$, is smooth around the points $(x^n_{j\pm}:=x_j\pm a^n_{j,k}\Delta t, y^n_{k\pm}:=y_k\pm a^n_{j,k}\Delta t)$; see Fig. 5.1. Therefore, the values of φ^{n+1} at these four points can be computed by the Taylor expansion

$$\varphi^{n+1}_{j\pm,k\pm}=\tilde\varphi\big(x^n_{j\pm},y^n_{k\pm},t^n\big)-\Delta t\cdot H\big(\tilde\varphi_x\big(x^n_{j\pm},y^n_{k\pm},t^n\big),\tilde\varphi_y\big(x^n_{j\pm},y^n_{k\pm},t^n\big)\big)+\mathcal{O}(\Delta t)^2. \tag{5.6}$$

Here, by complete analogy with our one-dimensional construction, the values of $\tilde\varphi(x^n_{j\pm}, y^n_{k\pm}, t^n)$ are computed from the corresponding polynomials (5.2) or (5.3), i.e., $\varphi^n_{j+,k+}=\tilde\varphi^{\mathrm{NE}}(x_{j+},y_{k+})$, $\varphi^n_{j+,k-}=\tilde\varphi^{\mathrm{SE}}(x_{j+},y_{k-})$, and so on. With $\lambda:=\Delta t/\Delta x$ and $\mu:=\Delta t/\Delta y$ being the fixed mesh ratios, we obtain

$$\begin{aligned}\varphi^n_{j\pm,k+}&=\varphi^n_{j,k}\pm\lambda a^n_{j,k}(\Delta\varphi)^n_{j\pm\frac12,k}+\mu a^n_{j,k}(\Delta\varphi)^n_{j,k+\frac12}+\frac{\lambda a^n_{j,k}\big(\lambda a^n_{j,k}-1\big)}{2}(\Delta\varphi)'_{j\pm\frac12,k}\\&\quad+\frac{\mu a^n_{j,k}\big(\mu a^n_{j,k}-1\big)}{2}(\Delta\varphi)^{\backprime}_{j,k+\frac12}\pm\frac{\lambda\mu\big(a^n_{j,k}\big)^2}{2}\Big((\Delta\varphi)'_{j,k+\frac12}+(\Delta\varphi)^{\backprime}_{j\pm\frac12,k}\Big),\\
\varphi^n_{j\pm,k-}&=\varphi^n_{j,k}\pm\lambda a^n_{j,k}(\Delta\varphi)^n_{j\pm\frac12,k}-\mu a^n_{j,k}(\Delta\varphi)^n_{j,k-\frac12}+\frac{\lambda a^n_{j,k}\big(\lambda a^n_{j,k}-1\big)}{2}(\Delta\varphi)'_{j\pm\frac12,k}\\&\quad+\frac{\mu a^n_{j,k}\big(\mu a^n_{j,k}-1\big)}{2}(\Delta\varphi)^{\backprime}_{j,k-\frac12}\mp\frac{\lambda\mu\big(a^n_{j,k}\big)^2}{2}\Big((\Delta\varphi)'_{j,k-\frac12}+(\Delta\varphi)^{\backprime}_{j\pm\frac12,k}\Big).\end{aligned} \tag{5.7}$$

The derivatives on the RHS of (5.6) are computed by plugging $(x^n_{j\pm}, y^n_{k\pm})$ into the derivatives of the corresponding polynomials (5.2),(5.3),

$$\begin{aligned}
\tilde{\varphi}_x\big(x^n_{j\pm}, y^n_{k+}, t^n\big) &= \frac{(\Delta\varphi)^n_{j\pm\frac12,k}}{\Delta x} \mp \left(\frac12 - \lambda a^n_{j,k}\right)\frac{(\Delta\varphi)'_{j\pm\frac12,k}}{\Delta x} + \lambda a^n_{j,k}\frac{(\Delta\varphi)'_{j,k+\frac12}}{2\Delta y}\\
&\quad + \mu a^n_{j,k}\frac{(\Delta\varphi)`_{j\pm\frac12,k}}{2\Delta x},\\
\tilde{\varphi}_x\big(x^n_{j\pm}, y^n_{k-}, t^n\big) &= \frac{(\Delta\varphi)^n_{j\pm\frac12,k}}{\Delta x} \mp \left(\frac12 - \lambda a^n_{j,k}\right)\frac{(\Delta\varphi)'_{j\pm\frac12,k}}{\Delta x} - \lambda a^n_{j,k}\frac{(\Delta\varphi)'_{j,k-\frac12}}{2\Delta y}\\
&\quad - \mu a^n_{j,k}\frac{(\Delta\varphi)`_{j\pm\frac12,k}}{2\Delta x},\\
\tilde{\varphi}_y\big(x^n_{j\pm}, y^n_{k+}, t^n\big) &= \frac{(\Delta\varphi)^n_{j,k+\frac12}}{\Delta y} - \left(\frac12 - \mu a^n_{j,k}\right)\frac{(\Delta\varphi)`_{j,k+\frac12}}{\Delta y} \pm \lambda a^n_{j,k}\frac{(\Delta\varphi)'_{j,k+\frac12}}{2\Delta y}\\
&\quad \pm \mu a^n_{j,k}\frac{(\Delta\varphi)`_{j\pm\frac12,k}}{2\Delta x},\\
\tilde{\varphi}_y\big(x^n_{j\pm}, y^n_{k-}, t^n\big) &= \frac{(\Delta\varphi)^n_{j,k-\frac12}}{\Delta y} + \left(\frac12 - \mu a^n_{j,k}\right)\frac{(\Delta\varphi)`_{j,k-\frac12}}{\Delta y} \pm \lambda a^n_{j,k}\frac{(\Delta\varphi)'_{j,k-\frac12}}{2\Delta y}\\
&\quad \pm \mu a^n_{j,k}\frac{(\Delta\varphi)`_{j\pm\frac12,k}}{2\Delta x}.
\end{aligned} \tag{5.8}$$

2. Projection. Finally, we project this computed solution back onto the original grid. Since the distance between the points (x_j, y_k) and $(x_{j\pm}, y_{k\pm})$ is proportional to $\mathcal{O}(\Delta t)$, we obtain a sufficiently accurate approximation to $\varphi(x_j, y_k, t^{n+1})$ by averaging the values of $\varphi^{n+1}_{j\pm,k\pm}$ computed at the previous step, (5.6)–(5.8). The resulting fully discrete scheme,

$$\begin{aligned}
\varphi^{n+1}_{j,k} &= \frac14\big(\varphi^{n+1}_{j+,k+} + \varphi^{n+1}_{j+,k-} + \varphi^{n+1}_{j-,k+} + \varphi^{n+1}_{j-,k-}\big) + \mathcal{O}(\Delta t)^2\\
&= \varphi^n_{j,k} + \frac{\lambda a^n_{j,k}}{2}\Big((\Delta\varphi)^n_{j+\frac12,k} - (\Delta\varphi)^n_{j-\frac12,k}\Big) + \frac{\mu a^n_{j,k}}{2}\Big((\Delta\varphi)^n_{j,k+\frac12} - (\Delta\varphi)^n_{j,k-\frac12}\Big)\\
&\quad + \frac{\lambda a^n_{j,k}\big(\lambda a^n_{j,k} - 1\big)}{4}\Big((\Delta\varphi)'_{j+\frac12,k} + (\Delta\varphi)'_{j-\frac12,k}\Big)\\
&\quad + \frac{\mu a^n_{j,k}\big(\mu a^n_{j,k} - 1\big)}{4}\Big((\Delta\varphi)`_{j,k+\frac12} + (\Delta\varphi)`_{j,k-\frac12}\Big)\\
&\quad - \frac{\Delta t}{4}\sum_{\pm} H\big(\tilde{\varphi}_x\big(x^n_{j\pm}, y^n_{k\pm}, t^n\big), \tilde{\varphi}_y\big(x^n_{j\pm}, y^n_{k\pm}, t^n\big)\big) + \mathcal{O}(\Delta t)^2,
\end{aligned} \tag{5.9}$$

is second-order accurate in space and only first-order in time. We note that obtaining $\varphi^{n+1}_{j,k}$ by averaging the intermediate values $\varphi^{n+1}_{j\pm,k\pm}$ creates a negligible error of order $\mathcal{O}(\Delta t)^2$. Indeed, this deviation vanishes later on as we take the semi-discrete limit $\Delta t \downarrow 0$.

As in the one-dimensional case, we now subtract $\varphi^n_{j,k}$ from both sides of (5.9), divide by Δt, and pass to the limit as $\Delta t \to 0$, obtaining the *second-order, semi-discrete,*

two-dimensional, central scheme,

$$\frac{d}{dt}\varphi_{j,k}(t) = -\frac{1}{4}[H(\varphi_x^+(t),\varphi_y^+(t))+H(\varphi_x^+(t),\varphi_y^-(t)) + H(\varphi_x^-(t),\varphi_y^+(t)) + H(\varphi_x^-(t),\varphi_y^-(t))] + \frac{a_{j,k}(t)}{2}[(\varphi_x^+(t)-\varphi_x^-(t))+(\varphi_y^+(t)-\varphi_y^-(t))]. \quad (5.10)$$

Here, the local speed $a_{j,k}(t)$ is given by (5.5), and all the quantities on the right are attached to the point (x_j, y_k), namely

$$\begin{aligned}\varphi_x^{\pm} &:= \tilde{\varphi}_x(x_j \pm 0, y_k, t) = \frac{(\Delta\varphi)_{j\pm\frac{1}{2},k}(t)}{\Delta x} \mp \frac{(\Delta\varphi)'_{j\pm\frac{1}{2},k}(t)}{2\Delta x},\\ \varphi_y^{\pm} &:= \tilde{\varphi}_y(x_j, y_k \pm 0, t) = \frac{(\Delta\varphi)_{j,k\pm\frac{1}{2}}(t)}{\Delta y} \mp \frac{(\Delta\varphi)'_{j,k\pm\frac{1}{2}}(t)}{2\Delta y}.\end{aligned} \quad (5.11)$$

Finally, to obtain the same second-order accuracy in time, our semi-discrete scheme, (5.10)–(5.11), should be complemented with at least second-order method for time discretization.

6. NUMERICAL EXAMPLES

We conclude the paper with a number of numerical examples. The numerical experiments presented below are based on our second-order semi-discrete schemes—(4.9)–(4.10) and (5.10)–(5.11) in the one- and two-dimensional cases, complemented with the θ-dependent limiter (2.2) with $\theta = 2$. The semi-discrete solution evolved in time using the second-order modified Euler method, computed with timestep $\Delta t = 0.475 \times \Delta t_{\text{CFL}}$, where Δt_{CFL} is the maximal timestep dictated by the CFL limitation.

6.1. One-dimensional Hamilton–Jacobi equation.

EXAMPLE 1. *Burgers-type equation.* First, consider the following periodic initial value problem,

$$\begin{cases}\varphi_t + H(\varphi_x) = 0,\\ \varphi(x,0) = -\cos(\pi x),\end{cases} \quad (6.1)$$

with a strictly convex (Burgers-type) Hamiltonian

$$H(p) = \frac{(p+1)^2}{2}, \quad (6.2)$$

or a non-convex Hamiltonian

$$H(p) = -\cos(p+1). \quad (6.3)$$

For both of these problems the singularity occurs at about $t = 1/\pi^2$. The approximate solutions at time $t = 1.5/\pi^2$, obtained by our second-order semi-discrete scheme, (4.9)–(4.10), are presented in Figs. 6.1–6.2. We observe both high-resolution and non-oscillatory behavior of our one-dimensional scheme.

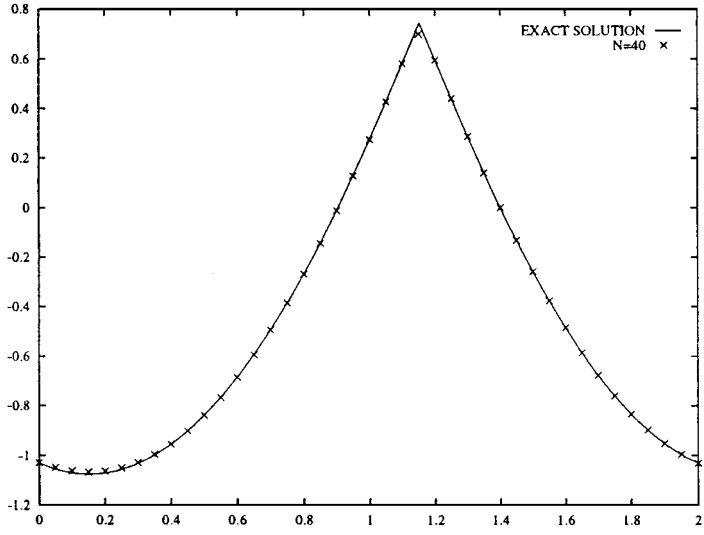

FIG. 6.1. Problem (6.1), (6.2).

EXAMPLE 2. *Riemann problem.* In this example we solve numerically the Riemann problem for a HJ equation with a non-convex Hamiltonian,

$$\begin{cases} \varphi_t + \frac{1}{4}\left(\varphi_x^2 - 1\right)\left(\varphi_x^2 - 4\right) = 0, \\ \varphi(x, 0) = -2|x|. \end{cases} \tag{6.4}$$

The numerical solution obtained by our second-order semi-discrete scheme is shown in Fig. 6.3. When the mesh is refined, this solution converges to the exact (viscosity) solution much faster than the solution computed by the LT scheme (Fig. 6.4). This is due to the fact that our new scheme, (4.9)–(4.10), has smaller numerical dissipation than the

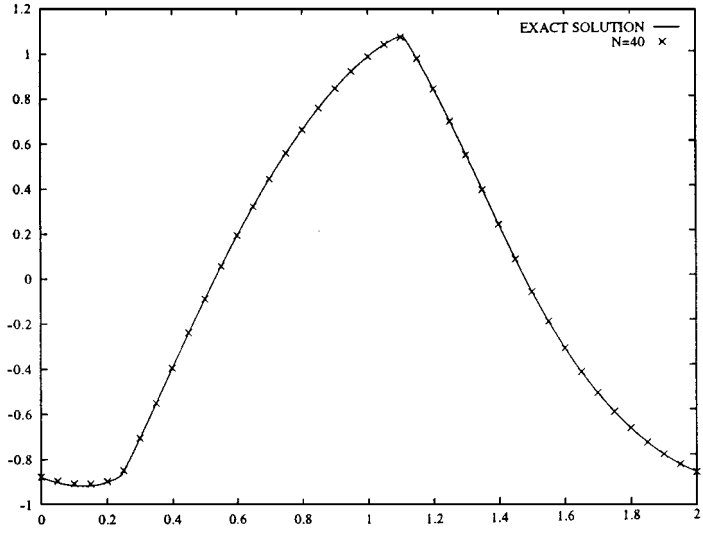

FIG. 6.2. Problem (6.1), (6.3).

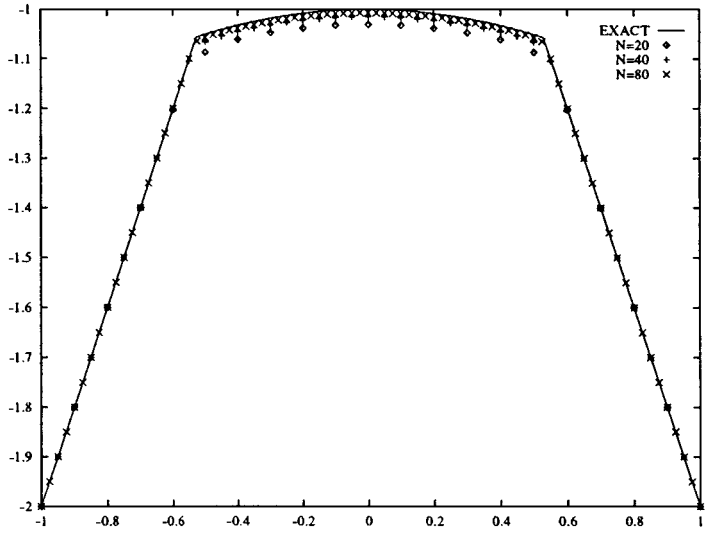

FIG. 6.3. Problem (6.4), $\mathbf{T = 1}$. Resolution via the new second-order scheme, (4.9)–(4.10).

LT scheme, particularly in the regions where $H'(\varphi_x) \ll 1$, i.e., near the maximum in this example.

6.2. Two-dimensional problems.

EXAMPLE 3. *Two-dimensional Hamilton–Jacobi equation.* Let us consider the following two-dimensional HJ equation with a convex Hamiltonian,

$$\varphi_t + \sqrt{\varphi_x^2 + \varphi_x^2 + 1} = 0, \tag{6.5}$$

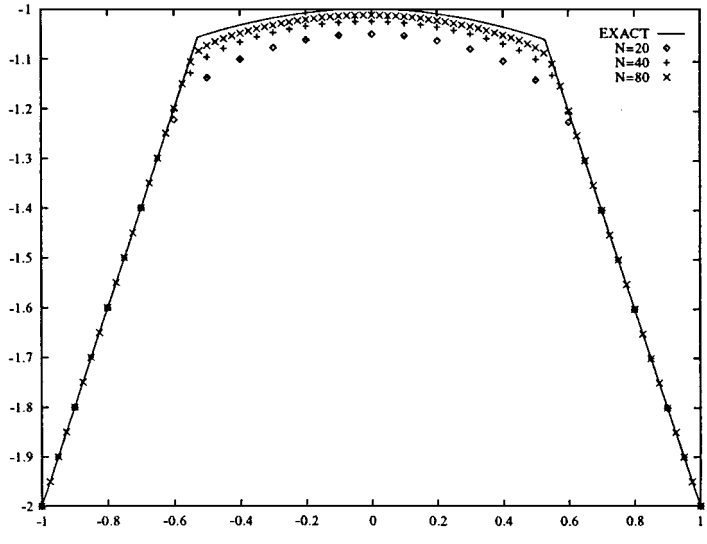

FIG. 6.4. Problem (6.4), $\mathbf{T = 1}$. Resolution via the second order LT scheme, (2.6)–(2.7).

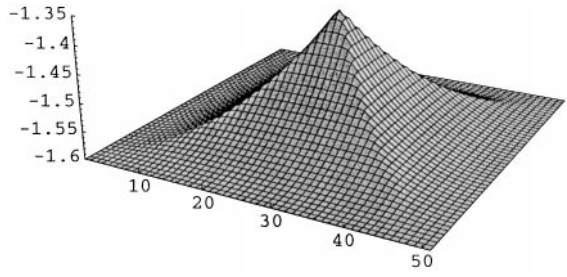

FIG. 6.5. Problem (6.5)–(6.6), Mesh, $50 * 50$.

which is a prototype model in geometrical optics. We solve this eikonal equation subject to the smooth periodic initial data,

$$\varphi(x, y, 0) = \frac{1}{4}(\cos(2\pi x) - 1)(\cos(2\pi y) - 1) - 1. \tag{6.6}$$

The numerical solution to this Cauchy problem, (6.5)–(6.6), at time $t = 0.6$ (after formation of the singularity) was computed by our two-dimensional second-order semi-discrete scheme, (5.10)–(5.11). We would like to stress its non-oscillatory nature and high resolution of the singularity; see Figs. 6.5, 6.6.

EXAMPLE 4. *Incompressible Euler and Navier–Stokes equations.* In this example we consider two-dimensional viscous and inviscid incompressible flow governed by the Navier–Stokes ($\nu > 0$) and Euler ($\nu = 0$) equations, respectively,

$$\omega_t + u\omega_x + v\omega_y = \nu\Delta\omega. \tag{6.7}$$

Here, $\mathbf{u} = (u, v)$ is the two-component divergence-free velocity field, satisfying

$$u_x + v_y = 0, \tag{6.8}$$

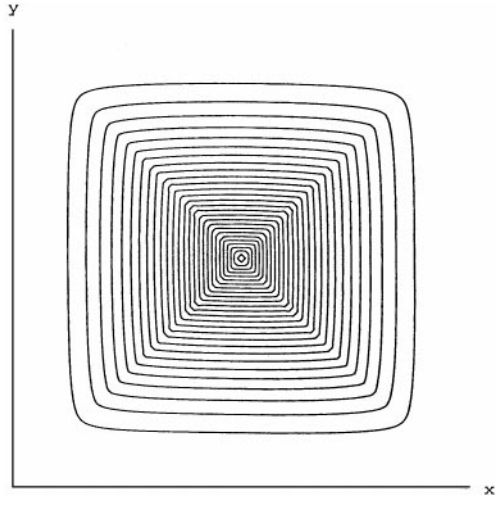

FIG. 6.6. Problem (6.5)–(6.6), Mesh, $100 * 100$.

and $\omega := v_x - u_y$ is the vorticity. This is a transport equation for the vorticity, which can be viewed as a two-dimensional viscous HJ equation with a *global* Hamiltonian, $H(\omega_x, \omega_y) := u\omega_x + v\omega_y$.

When applied to Eq. (6.7), our two-dimensional, second-order, semi-discrete scheme, (5.10)–(5.11), takes the form

$$\begin{aligned}\frac{d}{dt}\omega_{j,k}(t) = &-\frac{1}{2}[u_{j,k}(t)(\omega_x^+(t) + \omega_x^-(t)) + v_{j,k}(t)(\omega_y^+(t) + \omega_y^-(t))] \\ &+ \frac{a_{j,k}(t)}{2}[(\omega_x^+(t) - \omega_x^-(t)) + (\omega_y^+(t) - \omega_y^-(t))] + \nu L_{j,k}(t). \qquad (6.9)\end{aligned}$$

Here, the local speed is given by $a_{j,k}(t) = \sqrt{u_{j,k}^2(t) + v_{j,k}^2(t)}$, the derivatives on the right are

$$\omega_x^{\pm}(t) = \frac{(\Delta\omega)_{j\pm\frac{1}{2},k}(t)}{\Delta x} \mp \frac{(\Delta\omega)'_{j\pm\frac{1}{2},k}(t)}{2\Delta x}, \qquad \omega_y^{\pm}(t) = \frac{(\Delta\omega)_{j,k\pm\frac{1}{2}}(t)}{\Delta y} \mp \frac{(\Delta\omega)'_{j,k\pm\frac{1}{2}}(t)}{2\Delta y}, \qquad (6.10)$$

and $L_{j,k}(t)$ denotes the central difference approximation of the linear viscous term,

$$L_{j,k}(t) = \frac{\omega_{j+1,k}(t) - 2\omega_{j,k}(t) + \omega_{j-1,k}(t)}{(\Delta x)^2} + \frac{\omega_{j,k+1}(t) - 2\omega_{j,k}(t) + \omega_{j,k-1}(t)}{(\Delta y)^2}. \qquad (6.11)$$

To complete the transport step (6.9), the incompressible computations require that at every time step, one recovers the velocities, $\{u_{j,k}, v_{j,k}\}$, from the known values of the vorticity, $\{\omega_{j,k}\}$. This can be done in a variety of ways—consult [8, 12, 18] and the references therein for recent examples. Here we have used a stream-function, ψ, such that $\Delta\psi = -\omega$, which is obtained by solving the five-points Laplacian, $\Delta\psi_{j,k} = -\omega_{j,k}(t)$. Its gradient, $\nabla\psi$, then recovers the velocity field,

$$u_{j,k}(t) = \frac{\psi_{j,k+1} - \psi_{j,k-1}}{2\Delta y}, \qquad v_{j,k}(t) = -\frac{\psi_{j+1,k} - \psi_{j-1,k}}{2\Delta x}. \qquad (6.12)$$

Remark. Observe that in this way we retain the discrete incompressibility, namely the velocities computed in (6.12) satisfy

$$\frac{u_{j+1,k} - u_{j-1,k}}{2\Delta x} + \frac{v_{j,k+1} - v_{j,k-1}}{2\Delta y} = 0.$$

We start our numerical experiments by checking the accuracy of our scheme, (6.9)–(6.11). We consider the Navier–Stokes equations, (6.7)–(6.8) with $\nu = 0.05$, subject to the smooth periodic initial data,

$$u(x, y, 0) = -\cos x \sin y, \qquad v(x, y, 0) = \sin x \cos y, \qquad (6.13)$$

which was used in [5], with exact solution, $(u(x, y, t), v(x, y, t)) = e^{-2\nu t}(-\cos x \sin y, \sin x \cos y)$.

The approximate solution with different number of grid points was computed at time $t = 2$. The errors, measured in terms of vorticity in the L^∞-, L^1-, and L^2-norms are shown in Table I. In this context we mention the L^1-convergence theory presented in

TABLE I
Initial Value Problem (6.7)–(6.8), (6.13), ν = 0.05

Nx ∗ Ny	L^∞-error	Rate	L^1-error	Rate	L^2-error	Rate
32 ∗ 32	3.140e-02	—	6.419e-01	—	1.125e-01	—
64 ∗ 64	8.041e-03	1.97	1.473e-01	2.12	2.588e-02	2.12
128 ∗ 128	4.459e-03	0.85	3.473e-02	2.08	6.261e-03	2.05
256 ∗ 256	2.281e-03	0.97	8.313e-03	2.06	1.706e-03	1.88

Note. Errors at $T = 2$.

[19]. In [19] we advocated that it is the L^1-rather than the L^∞-norm which reveals the optimal convergence rate of second-order high-resolution schemes. The results reconfirm this conclusion, by illustrating the L^1-second-order accuracy of our new central HJ scheme.

The second-order semi-discrete scheme, (6.9)–(6.12), was implemented for a model problem taken from [3, 4]. First, we solve the Euler equations, (6.7)–(6.8) with $\nu = 0$, subject to the $(2\pi, 2\pi)$-periodic initial data,

$$u(x, y, 0) = \begin{cases} \tanh\left(\frac{1}{\rho}(y - \pi/2)\right), & y \le \pi, \\ \tanh\left(\frac{1}{\rho}(3\pi/2 - y)\right), & y > \pi, \end{cases} \qquad v(x, y, 0) = \delta \cdot \sin(x). \tag{6.14}$$

Here, the "thick" shear-layer width parameter $\rho = \frac{\pi}{15}$ and the perturbation parameter $\delta = 0.05$.

The numerical results with 64×64 and 128×128 grids are presented using contour plots of ω in Figs. 6.7–6.8, and their corresponding two-dimensional configuration in, respectively, Figs. 6.9–6.10. Our results offer improved resolution when compared with the results of the corresponding fully discrete central scheme of Levy and Tadmor [18], which is

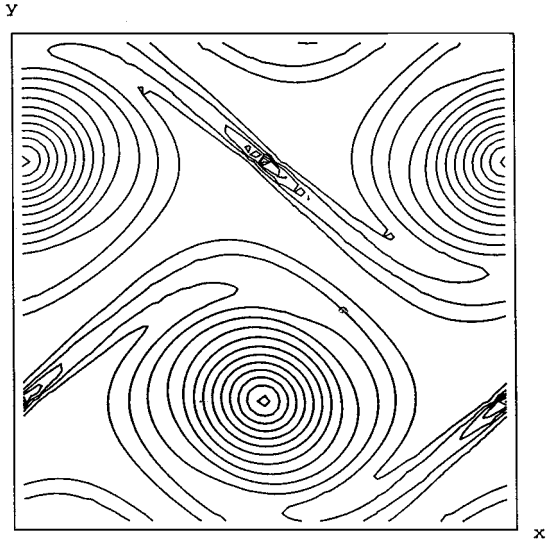

FIG. 6.7. Euler; **T = 10**, 64 ∗ 64 grid.

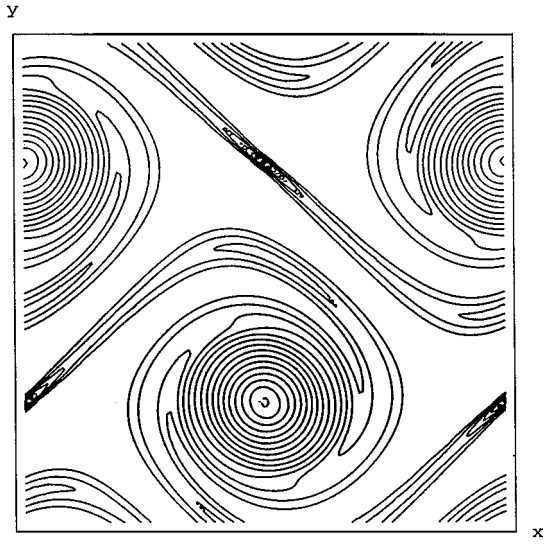

FIG. 6.8. Euler; $\mathbf{T} = \mathbf{10}$, $128 * 128$ grid.

based on the *conservative* formulation of the inviscid vorticity equation $\omega_t + \nabla \cdot (\mathbf{u}\omega) = 0$. Indeed, the resolution of the second-order results in Figs. 6.7–6.10 lies in between the second- and third-order versions used in [18, Figs. 6.6–6.7] and Figs. 6.12–6.13]. The improved resolution is attributed to the smaller amount of numerical dissipation present in our scheme. This can be clearly seen when comparing the corresponding extrema values: the maximal value of the solution computed by (6.9)–(6.12) is $\sim$4.8 (Fig. 6.10), which is larger than the maximal value of $\sim$2.8 due to the increased amount of dissipation present in the corresponding second-order Levy–Tadmor solution [18, Fig. 6.7]. At the same time we observe that the solution depicted in Figs. 6.8, 6.10 has spurious spikes, whereas the corresponding results in [18] are free of such oscillations. In this context we recall that the conservative solution satisfies a local maximum principle [18, Theorem 4.1], which hinges on an appropriate discrete incompressibility outlined in [18, 3.7]. A analogous discrete

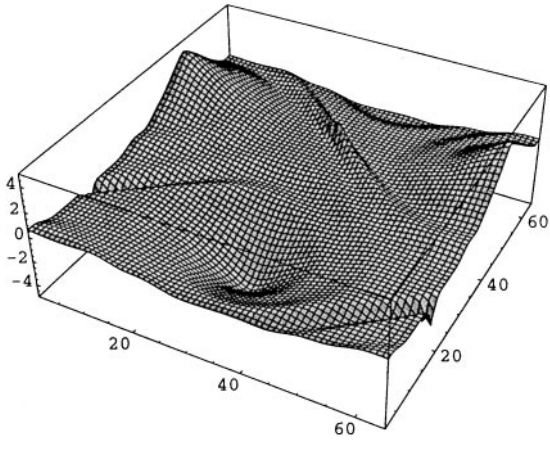

FIG. 6.9. Euler; $\mathbf{T} = \mathbf{10}$, $64 * 64$ grid.

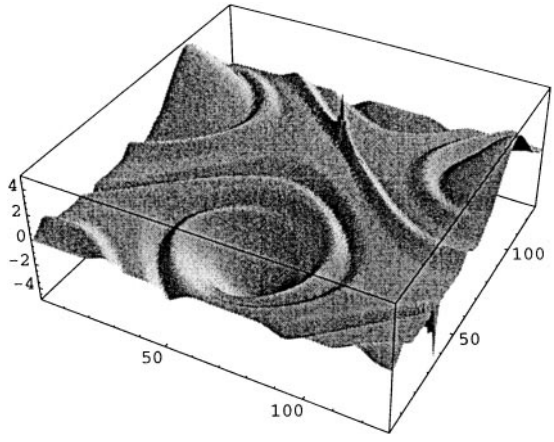

FIG. 6.10. Euler; $\mathbf{T} = \mathbf{10}$, $128 * 128$ grid.

incompressibility which would prevent the formation of spurious spikes is sought for our central scheme.

Finally, we solve the Navier–Stokes (N-S) equations, (6.7)–(6.8) with $\nu = 0.01$, augmented with the so called "thick" shear-layer periodic initial data, (6.14), with $(\rho, \delta) = (\pi/50, 0.05)$.

The numerical results at time $t = 10$ with different numbers of grid points are presented in Figs. 6.11–6.14. The smallest scale in the two-dimensional NS equations is given by $\eta_{min} \sim \sqrt{\nu/\|\omega_0\|_\infty)}$, consult [11]. In the present case, $\eta_{min} \sim \sqrt{\nu \cdot \delta} \sim 10^{-2}$, so that the results in Figs. 6.11–6.12 with $N = 64$ and $N = 128$ grid points resolve the solution.

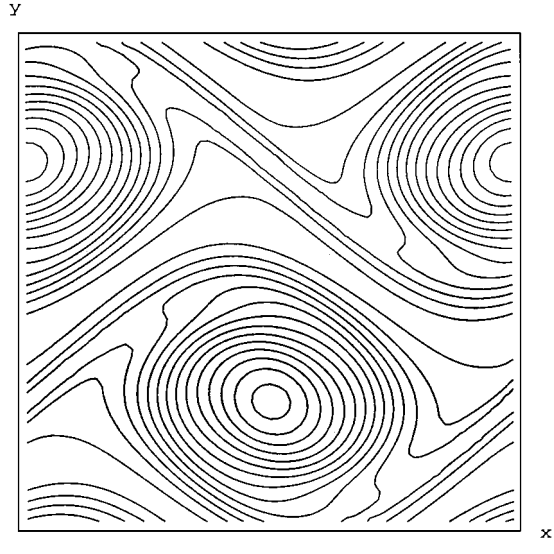

FIG. 6.11. N-S; $\mathbf{T} = \mathbf{10}$, $64 * 64$ grid.

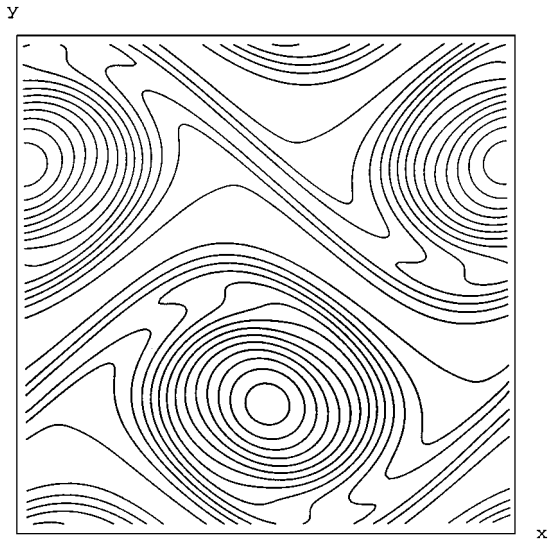

FIG. 6.12. N-S; $\mathbf{T} = \mathbf{10}$, $128 * 128$ grid.

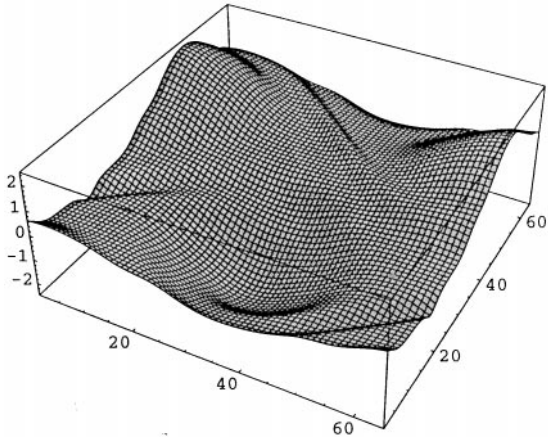

FIG. 6.13. N-S; $\mathbf{T} = \mathbf{10}$, $64 * 64$ grid.

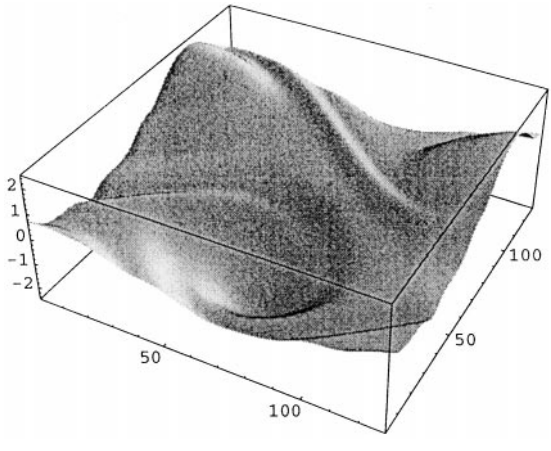

FIG. 6.14. N-S; $\mathbf{T} = \mathbf{10}$, $128 * 128$ grid.

ACKNOWLEDGMENTS

The work of A. Kurganov was supported in part by the NSF Group Infrastructure Grant. The work of E. Tadmor was supported in part by NSF Grant DMS97-06827 and ONR Grant N00014-91-J-1076.

REFERENCES

1. R. Abgrall, Numerical discretization of first-order Hamilton–Jacobi equation on triangular meshes, *Comm. Pure Appl. Math.* **49**, 1339 (1996).
2. M. Bardi, M. Crandall, L. Evans, H. Sonar, and P. Souganidis, Viscosity solutions and applications, in *CIME Lecture Notes*, edited by I. Capuzzo Dolcetta and P.-L. Lions, Lecture Notes in Mathematics (Springer-Verlag, New York/Berlin, 1997), Vol. 1660.
3. J. B. Bell, P. Colella, and H. M. Glaz, A second-order projection method for the incompressible Navier–Stokes equations, *J. Comput. Phys.* **85**, 257 (1989).
4. D. L. Brown and M. L. Minion, Performance of under-resolved two-dimensional incompressible flow simulations, *J. Comput. Phys.* **122**, 165 (1995).
5. A. Chorin, Numerical solution of the Navier–Stokes equations, *Math. Comp.* **22**, 745 (1968).
6. L. Corrias, M. Falcone, and R. Natalini, Numerical schemes for conservation laws via Hamilton–Jacobi equations, *Math. Comp.* **64**, 555 (1995).
7. M. G. Crandall and P.-L. Lions, Two approximations of solutions of Hamilton–Jacobi equations, *Math. Comp.* **43**, 1 (1984).
8. W. E and J.-G. Liu, Finite difference schemes for incompressible flows in the velocity-impulse density formulation, *J. Comput. Phys.* **130**, 67 (1997).
9. A. Harten, High resolution schemes for hyperbolic conservation laws, *J. Comput. Phys.* **49**, 357 (1983).
10. A. Harten, B. Engquist, S. Osher, and S. R. Chakravarthy, Uniformly high order accurate essentially non-oscillatory schemes, III, *J. Comput. Phys.* **71**, 231 (1987).
11. W. Henshaw, H.-O. Kreiss, and L. Reyna, Smallest scale for the incompressible Navier–Stokes equations, *Arch. Rat. Mech. Anal.* **112**, 21 (1990).
12. T. Y. Hou and B. T. R. Wetton, Second-order convergence of a projection scheme for the incompressible Navier–Stokes equations with boundaries, *SINUM* **30**(3), 609 (1993).
13. C. Hu and C.-W. Shu, A discontinuous Galerkin finite element method for Hamilton–Jacobi equations, preprint.
14. A. Kurganov, *Conservation Laws: Stability of Numerical Approximations and Nonlinear Regularization*, Ph.D. Thesis, Tel-Aviv University, Israel, 1997.
15. A. Kurganov and E. Tadmor, New high-resolution central schemes for nonlinear conservation laws and convection-diffusion equations, *J. Comput. Phys.*, in press.
16. G. Kossioris, Ch. Makridakis, and P. E. Souganidis, Finite volume schemes for the Hamilton–Jacobi equations, *Numer. Math.* **83**, 427 (1999).
17. B. van Leer, Towards the ultimate conservative difference scheme. V. A second order sequel to Godunov's method, *J. Comput. Phys.* **32**, 101 (1979).
18. D. Levy and E. Tadmor, Non-oscillatory central schemes for the incompressible 2-D Euler equations, *Math. Res. Lett.* **4**, 1 (1997).
19. C.-T. Lin and E. Tadmor, L^1-stability and error estimates for approximate Hamilton–Jacobi solutions, *Numer. Math.*, in press.
20. C.-T. Lin and E. Tadmor, High-resolution non-oscillatory central schemes for Hamilton–Jacobi equations, *SIAM J. Sci. Comput.*, in press.
21. H. Nessyahu and E. Tadmor, Non-oscillatory central differencing for hyperbolic conservation laws, *J. Comput. Phys.* **87**, 408 (1990).

22. S. Osher and C.-W. Shu, High-order essential nonoscillatory schemes for Hamilton–Jacobi equations, *SIAM J. Numer. Anal.* **28**, 907 (1991).
23. S. Osher and E. Tadmor, On the convergence of difference approximations to scalar conservation laws, *Math. Comp.* **50**, 19 (1988).
24. P. E. Souganidis, Approximation schemes for viscosity solutions of Hamilton–Jacobi equations, *J. Differential Equations* **59**, 1 (1985).
25. C.-W. Shu, Total-variation-diminishing time discretizations, *SISSC* **6**, 1073 (1988).
26. C.-W. Shu and S. Osher, Efficient implementation of essentially non-oscillatory shock-capturing schemes, *J. Comput. Phys.* **77**, 439 (1988).